during measurements of stationary PL spectra [4] the position of the maximum of a nonuniformly broadened line under the filling of pores by dielectric liquids shifts to the 'blue' side. This is apparently not due to a decrease in E_{exc}, but because of a decrease in the relaxation time of nonequilibrium charge carriers mainly in nanostructures that contribute to the low-energy part of the PL spectrum (see Section 4.4).

4.4 PL and FCA signal kinetics for PS in a dielectric ambience

Experiments have shown that the bleeding-in of a saturated vapor of benzene does not significantly affect the PL signal relaxation in PS (see Figs 4 and 6). This accords with the concepts considered in Section 2. Indeed, the dielectric constant of benzene is small and apparently the ratio of free charge carriers to those coupled in excitons does not vary significantly [see equation (7)]. Rather unexpectedly, at first glance, was the effect of the change of kinetic characteristics of PL and FCA after the filling of pores with mediums possessing high values of ε_d. The decrease of the radiative recombination efficiency was accompanied not by a growth, but by a decrease in the PL and FCA signal relaxation times (see Figs 4 and 6). In the case of PL the effect was more pronounced for the long-wave parts of the spectrum corresponding to the contribution of nanostructures with larger cross sections (see Fig. 4). For all parts of the PL spectrum a decrease in the parameter β was observed, which indicates an increase in the degree of inhomogeneity of the PS nanostructure system.

The changes in the kinetic parameters of PL and FCA observed after the filling of pores with mediums featuring a high value of ε_d can be explained in the framework of the model considered as follows. The small efficiency of PL in the PS samples studied obviously implies the following relation between the radiative and nonradiative recombination times: $\tau_r \geqslant \tau_{nr}$. This relation is enhanced for nanostructures with larger diameters due to an increase of τ_r [5, 6]. Therefore, for just such structures, in accordance with equations (7), the relative decrease in exciton concentration must cause a decrease of the PL and FCA signal relaxation times. In the measurements of FCA, it is impossible to separate the contributions from nanostructures with different sizes, so we fix some average time τ_{FC}, but for PL the effect of the dependence of the τ_{PL} relative change on wavelength, predicted by the model, is registered quite well (see Fig. 4).

5. Conclusions

In the present paper a model for recombination processes in silicon nanostructures is developed, which assumes the presence of dynamically coupled subsystems at room temperature: free charge carriers and excitons. The data obtained for PS by time-resolved measurements of photoluminescence and free carrier absorption can be explained by the model proposed. In particular, the temperature behaviour of the PL and FCA signals, as well as the dependences of the amplitude and temporal characteristics of these signals on the dielectric properties of the ambience around the quantum wires of the PS, are in full agreement with the model's predictions.

This work was supported financially by the State Scientific and Technical Programs: 'Physics of Solid-State Nanostructures' (project 1-066/3) and 'Atomic Surface Structures' (project 96-1.33).

References

1. Uhlir A *Bell Syst. Techn.* **35** 333 (1956)
2. Bomchil G, Halimaoui A, Herino R *Appl. Surf. Sci.* **41/42** 604 (1989)
3. Cullis A G, Canham L T, Calcott P D J *J. Appl. Phys.* **82** 909 (1997)
4. Kashkarov P K, Konstantinova E A , Timoshenko V Yu *Fiz. Tekh. Poluprovodn.* **30** 1479 (1996) [*Semiconductors* **30** 778 (1996)]
5. Sanders G D, Chang Y-C *Phys. Rev. B* **45** 9202 (1992)
6. John G C, Singh V A *Phys. Rep.* **263** 93 (1995)
7. Babichenko V S, Keldysh L V, Silin A P *Fiz. Tverd. Tela* **22** 1238 (1980) [*Sov. Phys. Solid. State* **22** 723 (1980)]
8. Kashkarov P K et al. *Phys. Low-Dim. Struct.* (1/2) 123 (1997)
9. Yassievich I N *Semicond. Sci. Technol.* **9** 1433 (1994)
10. Maly P et al. *Phys. Rev. B* **54** 7929 (1996)
11. Andryushin E A, Silin A P *Fiz. Tverd. Tela* **35** 1947 (1993) [*Phys. Solid. State* **35** 971 (1993)]

PACS number: **94.20.–y**

The atmospheric electric field as a source of variability in the ionosphere

S A Pulinets, V V Khegaĭ,
K A Boyarchuk, A M Lomonosov

1. Introduction

The terrestrial ionosphere is very sensitive to exposure to external factors, so its characteristics are subjected to regular and irregular variations. Ordinarily, the regime of the ionosphere is considered solely in connection with solar and cosmic effects [1]. However, some studies indicate that short-term anomalous variations appear in the ionosphere even under the constancy of external factors [2]. It is natural to suppose that the reason for these variations is internal, i.e. the ionosphere also reacts to the processes occurring in the troposphere and on the surface of the Earth. Volcanic activity, earthquakes, cyclones, thunder storms, explosions, various contaminations in the troposphere — all of them have an effect on the ionosphere. At present, this problem is being actively studied since there is experimental evidence for this relation [3, 4]. The results of these studies open up the prospect of constructing a self-consistent model for the electrodynamic interaction between the troposphere and ionosphere.

The purpose of the present paper is to study one possible mechanism for the influence of geological and anthropogenic factors on tropospheric and ionospheric processes resulting from electrostatic fields.

2. Tropospheric processes

Consider some processes changing the gradient of the electrostatic potential of the Earth in the troposphere.

2.1 Dust and sand storms

Dust has an effect on the atmospheric electric field, since the attachment of small ions and friction result in the dust particles acquiring an electric charge. It is established that most of large ions is negatively charged and that bigger aerosol particles seem to absorb negative ions more easily [5]. As noted in paper [6], during dust storms the maximal deviation of the atmospheric electric-field-potential gradient from the unperturbed value ranged from +15 to

-10 kV m^{-1} and the atmospheric space charge was a few times larger than during quiet weather ($\sim 10^5$ e cm^{-3}). Thus, near the surface a dense layer with a large uncompensated charge is formed which may affect the electric field gradient.

2.2 Volcanic activity

Volcano eruptions inject a large amount of ash and other particles into atmosphere. The net result is very similar to a dust storm, but at much higher altitudes. So it is not surprising that during volcano eruptions one may observe a genuine thunder storm caused by the uncompensated charge of the ash cloud. The big electric charge of ash is the reason for such volcanic thunder storms [7].

2.3 Radioactive contamination

The dust begins to play a special role when it becomes radioactive, for example, as a result of an accident at a nuclear plant, and has a strong effect on the atmospheric electric field strength. Here two possibilities for the formation of an anomalous electric field should be distinguished: firstly, the injection of a large number of radioactive particles at significant altitudes ($\sim 1-2$ km) as the result of the explosion; secondly, the deposition of radioactive species over a large area around the accident site. In the latter case the radioactivity acts over a narrow ($\sim 1-3$ m) near-surface layer (however, atmospheric processes can increase the height of this layer up to 300 m, for example, due to wind elevation), and the anomalous field is formed immediately near the Earth's surface. For instance, inside the 30-km isolation zone around the Chernobyl Atomic Power Station the ion production rate was 10^5-10^6 cm^{-3} s^{-1} practically everywhere within the total near-surface atmospheric layer (50 – 100 m). Due to the high density of the soil contaminants, the ion formation rate has not been subjected to short-term variations [8, 9].

2.4 Earthquakes

Perturbations of the near-surface vertical electrostatic field of the order of 50 – 150 V m^{-1} are often observed before earthquakes and violent volcano eruptions, and they amount to > 1000 V m^{-1} before catastrophic earthquakes. In papers [10, 11], a decrease or even a change of sign of the electric field vertical component were reported to occur a few hours before strong earthquakes. The earthquake epicentres are usually located near cracks in the Earth's crust, through which a significant amount of 'metallic' aerosols and radon, being a primary source of α-particles, emanates into the near-surface atmospheric layer [12, 13]. It is radon that is the main contributor to the ionization of the near-surface air. Each ^{222}Rn α-particle carrying a mean energy $E_\alpha = 6$ MeV can theoretically produce about 2×10^5 electron-ion pairs. According to experimental data, the outburst of radon before an earthquake can reach 12 eman corresponding to an ion production rate $Q \sim 7.6\times 10^3$ cm^{-3} s^{-1}. Products of the decay behave as light ions: they recombine to form molecular complexes with water, at least while they carry electric charge [14].

3. Theoretical model of the formation of the electric field near the Earth's surface

All the phenomena considered above lead, in one or another way, to the same result — the formation of a near-surface ionized layer. The difference is in the rate of charged particle production and in the thickness of the ionized layer. When radon comes out of the soil into the surface, only a thin layer (1 – 3 m) of the near-surface air is ionized [15], while during a dust storm or radioactive contamination it is necessary to consider a thicker layer (up to 300 m), since turbulent fluxes lift the radioactive soil particles high up above the surface. In the case of volcano eruption or radioactive ejection during an accident, the ionized layer can reach altitudes of up to 1 – 2 km above the surface.

Thus, many atmospheric particles become electrically charged under the action of radiation and as a result of friction and ion adsorption on atmospheric aerosols near the Earth's surface. All of them participate in different ion-molecular reactions characteristic of the near-surface air layer, which lead to *the formation of a stable composition of elementary ions and charged aerosols within the near-surface atmospheric layer* [16 – 18]. An uncompensated space charge is formed near the surface under the action of the natural atmospheric electric field E on ions of opposite signs due to their different mobilities [8]. This field makes the positive ions move downward to the surface and negative ones upward. In this way a near-surface 'electrode layer' is produced with a local field E_1 compensating for the main field $E - E_1$, which is shown schematically in Fig. 1. The field is lowered at the formation site of this layer. The field enhances above this layer due to the presence of a significant uncompensated space negative charge. A detailed model of this effect is considered in papers [19, 20]. Turbulent and regular action of air masses can spread this space charge over the thickness of the atmosphere thereby producing an anomalous electrode layer over large areas.

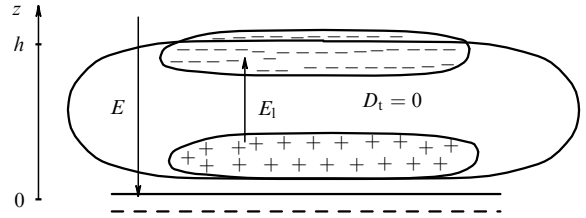

Figure 1.

The equations describing the kinetics of this system can be written in the form

$$\frac{\partial n_1}{\partial t} = \frac{\partial}{\partial z}\left[(D_t + D_1)\frac{\partial n_1}{\partial z}\right] - \mu_1\frac{\partial}{\partial z}(En_1) + q - \alpha n_1 n_2\,,$$

$$\frac{\partial n_2}{\partial t} = \frac{\partial}{\partial z}\left[(D_t + D_2)\frac{n_2}{\partial z}\right] + \mu_2\frac{\partial}{\partial z}(En_2) + q - \alpha n_1 n_2\,,$$

$$\frac{\partial E}{\partial z} = 4\pi e(n_1 - n_2)\,. \qquad (3.1)$$

Here e is the electron charge; z is the vertical coordinate (the layer is assumed to be infinite in the horizontal plane so the problem becomes essentially one-dimensional); n_1, n_2 are the concentrations of positive and negative ions; q is the ion production rate whose spatial distribution is well considered to be exponentially decaying: $q = q_0\exp(-z/h)$, where h is the ionized layer height; $\mu_{1,2}$ and $D_{1,2}$ are the mobilities and diffusion coefficients of the corresponding ions. The turbu-

lent diffusion coefficient is determined according to Ref. [21]:

$$D_t = (Kz + \gamma)(z + \beta)^{-1},$$

where $\beta = 10$ m, $\gamma = 5 \times 10^{-5}$ m^3 s^{-1}, K is the turbulence coefficient, and α is the ion recombination coefficient equal to $\sim 10^{-6}$ cm^3 s^{-1} [17].

We set the boundary conditions for the problem as follows: the electric field strength at the Earth's surface is $E_{z=0} = -100$ V m^{-1}, and at the boundary of the layer considered is $\partial E/\partial z|_{z=\infty} = 0$. We assume the initial concentrations of positive and negative charges to be equal a background value of ~ 450 cm^{-3}.

The calculated results of this model are presented in Fig. 2a,b, where the concentrations of positive and negative ions and the electrostatic field profile are plotted as functions of altitude 50 s after the ionization has begun (the moment of radon emerging at the surface). The formation of the near-surface electrode layer with a sharp field drop is clearly seen in the figure. The field grows significantly above this layer. The effect is enhanced by increasing the mobility and changing the diffusive behaviour of ions. It should also be taken into account that ions of both signs are removed from the ion production region under the action of the external field E, and since the collision of two oppositely charged ions is needed for ions to recombine, the resulting recombination slows down and ion storage takes place near the region boundary. This in turn may enhance the effect. The presence of a metallic aerosol flux increases the space negative charge and strengthens the field above the electrode layer, as seen in Fig. 2b.

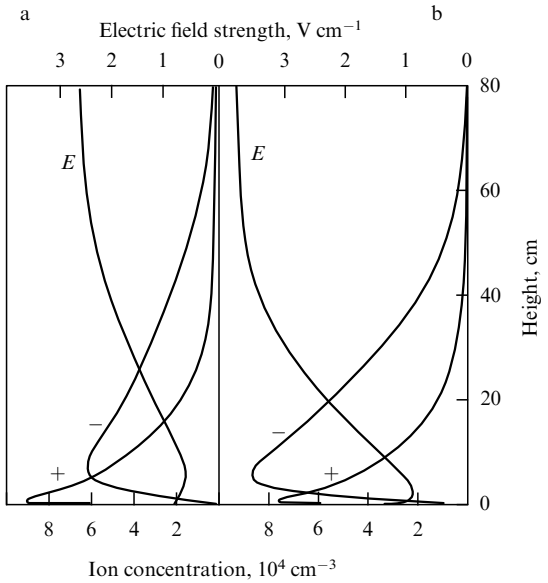

Figure 2.

The small ions are more mobile than big ones but they are very rapidly adsorbed onto aerosol particles thus forming large ions which are less subject to drift due to the electric field [22, 23]. In a bipolar atmosphere this process, however, can give rise to unexpected electric effects caused by charge separation mechanisms different from those considered above. In particular, the Earth's gravity acts more strongly on heavy aerosol particles. In this way by adsorbing light ions of different signs they may cause an appreciable space charge redistribution in the atmosphere which is impossible when the light ion drift is due only to the Earth's natural field. Drops of water in the cloud may play the role of heavy aerosol particles. The presence of an ionization source in the cloud due to convective processes can lead to a significant space charge separation caused by the transfer of oppositely charged ions by water drops. These effects are characteristic of radioactive injection after an accident or volcano eruption since these processes are accompanied by the outburst of an appreciable quantity of vapor and aerosol particles to altitudes more than 1–2 km.

The theory of charge separation by water drops in thunderclouds was elaborated by Wilson [24]. A falling drop (or ice crystal) in the Earth's natural field acquires an induced dipole moment: the positive charge is at the bottom, the negative one at the top. Since in the cases under consideration large complex ions with low mobility are present and continually generated in the air (fast small ions will have no noticeable effect and electrons may be neglected because of their low concentration in the troposphere), the falling drop will accumulate a negative charge by attracting negative ions and repelling positive ones. A positive ion may approach the drop from above, but the high velocity of the drop's fall makes this process improbable. Thus the drop accumulates a negative charge which is transferred to the bottom part of the cloud.

Both upgoing and downgoing convective streams of water drops and ice crystals exist in the cloud, so one may also suppose that small drops carried along by the upgoing convective stream will carry positive charge upwards in a like manner.

To describe these processes we need to change system of equations (3.1) by adding terms that describe the kinetics of the interaction of charged and neutral aerosol particles with light ions [23] and take into account the upgoing and downgoing jet streams.

The results of calculations with the modified system of equations are shown in Fig. 3. The positive and negative ion concentrations and electric field distributions are shown for a

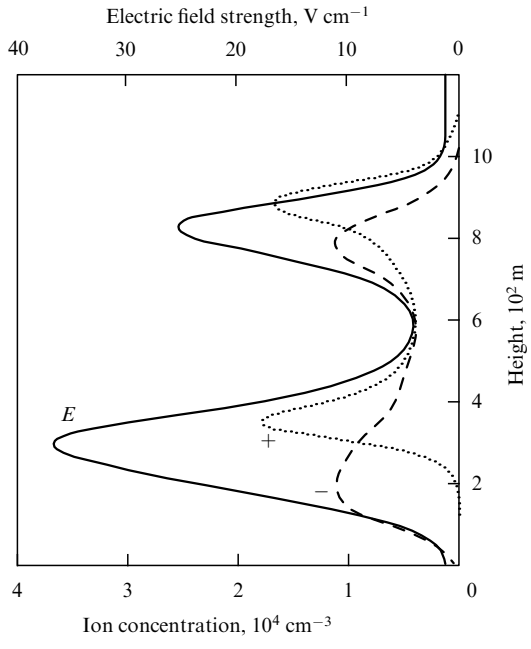

Figure 3.

cloud with enhanced ionization at an altitude of ~ 1 km. The ionization rate here is about 10^4 cm^{-3} s^{-1}. In this case the principal charge separation mechanism is the transfer of negative charge downward by falling drops and of positive charge upward as in the thundercloud cell model [24]. Such a process can lead to a strong field change over a wide range $\pm$ 5 kV m^{-1}. By this means, the theoretical model gives rise to the possibility of anomalous electric field establishment over large areas under various meteorological conditions.

4. Ionospheric effects

4.1 Penetration of the electric field into the ionosphere

The problem of electric field penetration into the ionosphere and related effects have been considered in many papers. In particular, in Refs [25, 26] the problem of electric field penetration from the E-region into the F-region and from the troposphere into the ionosphere, respectively, have been studied.

Let us calculate the penetration of a horizontally localized vertical electrostatic field into the ionosphere for the case considered. We choose a cylindrical reference frame (r, φ, z). Let the distribution of the vertical electrostatic field strength E_z on a fixed base plane $z_0 = \text{const}$ above the Earth's surface (for example, above the upper boundary of the electrode layer in a region with enhanced ionization) be Gaussian-like as shown in Fig. 4. The field strength decrease with distance from the localization centre can be represented in the form

$$E_z = E_0 \exp\left[-d\left(\frac{r}{a}\right)^2\right],$$

where E_0 is the maximum value of E_z; $d = 4\ln(10)$; a is the characteristic size of the field localization region, specifically, the diameter of the enhanced ionization region.

To determine the field at ionospheric altitudes, we shall use the approach developed in paper [26]. Assuming a horizontal stratification of the medium and a vertical geomagnetic field, it is easy to deduce the following equation for electric potential ϕ from the equation of continuity for the current:

$$\frac{\partial^2}{\partial r^2}\phi + \frac{1}{r}\frac{\partial}{\partial r}\phi + \frac{1}{\sigma_1}\frac{\partial}{\partial z}\left(\sigma_0\frac{\partial}{\partial z}\phi\right) = 0.$$

Here σ_1 is the Pedersen conductivity, and σ_0 is the conductivity along the geomagnetic field.

The distribution of the conductivities with altitude can be given as follows: $\sigma_0 = \sigma_1 = b\exp(z/h)$ for $0 \leqslant z \leqslant z_1$, $\sigma_{0,1} = b_1\exp[(z - z_1)/h_{0,1}]$ for $z_1 \leqslant z \leqslant z_2$, where $z_2 = 90$ km, $z_1 = 50$ and 65 km for day and night conditions, respectively; $h = 6.5$ km; $h_0 = 3$ km; $h_1 = 4.5$ km; $b = 2\times 10^{-13}$ Mo m^{-1}; $b_1 = b\exp(z_1/h)$. Such a distribution of $\sigma_{0,1}$ roughly corresponds to the empirical model for conductivity [27] shown in Fig. 5. In this case the general solution to the equation for the electric potential ϕ can be represented in the form

$$\phi(0 \leqslant z \leqslant z_1) = \int_0^\infty J_0(kr)\left[A_1(k)\exp(c_1 z) + B_1(k)\exp(c_2 z)\right]\mathrm{d}k,$$

$$\phi(z_1 \leqslant z \leqslant z_2) = \int_0^\infty J_0(kr)\left[A_2(k)I_v(kf) + B_2(k)K_v(kf)\right]f^v\,\mathrm{d}k,$$

where

$$c_1 = -\frac{1}{2h} - \left(\frac{1}{4h^2} + k^2\right)^{1/2}, \quad c_2 = -\frac{1}{2h} + \left(\frac{1}{4h^2} + k^2\right)^{1/2},$$

$$v = \frac{h_1}{h_1 - h_0}, \quad f = \frac{2h_1 h_0}{h_1 - h_0}\exp\left[-\frac{h_1 - h_0}{2h_1 h_0}(z - z_1)\right].$$

Here J_0 is the Bessel function of zeroth order; I_v and K_v are the modified Bessel functions of the first and second kind, respectively, and A_1, B_1, A_2, B_2 are numerical coefficients. Above the altitude $z = z_2 = 90$ km the force lines can be considered equipotential, as shown in Fig. 4, so the distribution of ϕ for $z > z_2$ is the same as at $z = z_2$. From here we obtain that the electric field of the source of the localized field in ionosphere at altitudes $z \geqslant 90$ km is determined by the relation

$$E_r = -\frac{\partial}{\partial r}\phi\Big|_{z=z_2} = \int_0^\infty J_1(kr)\left[A_2(k)I_v(kf|_{z=z_2}) + B_2(k)K_v(kf|_{z=z_2})\right]f^v|_{z=z_2}\,k\,\mathrm{d}k,$$

where J_1 is the Bessel function of the first order, and the coefficients A_1, B_1, A_2, B_2 can be found from the boundary

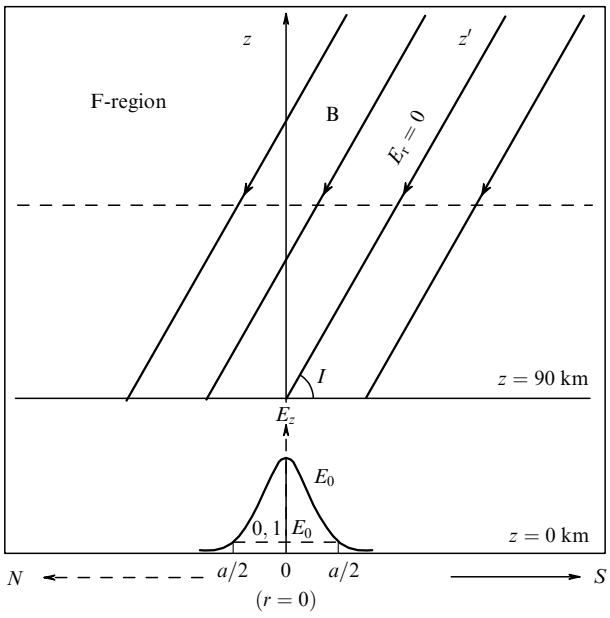

Figure 4.

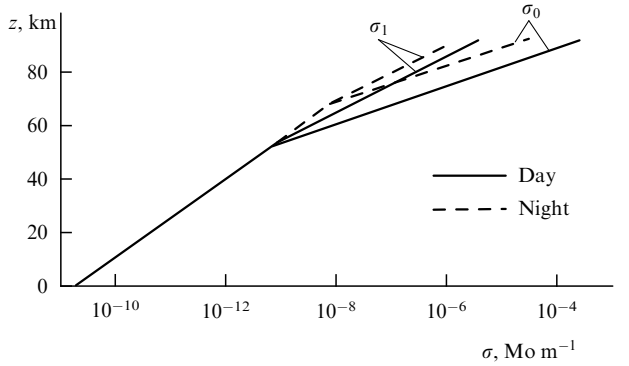

Figure 5.

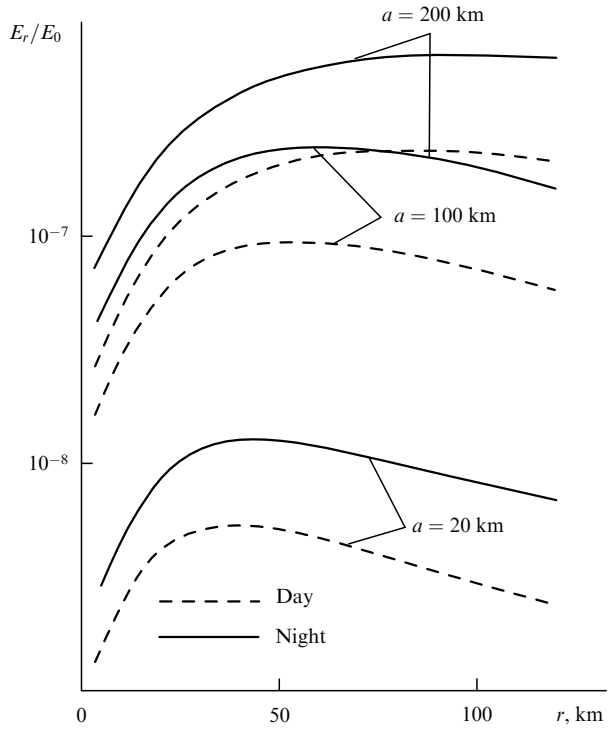

Figure 6.

conditions to the problem:

$$-\frac{\partial}{\partial r}\phi\Big|_{z=0} = E_0 \exp\left[-d\left(\frac{r}{a}\right)^2\right],$$

and from the continuity of ϕ at $z = z_1$; $(\partial/\partial z)\phi|_{z=z_2} = 0$.

The results of calculations of the ionospheric distribution for the horizontal field strength E_r normalized by E_0 for various sizes of the field localization region E_z during the day and night are shown in Fig. 6. It is seen that during the day the degree of field penetration into the ionosphere is much smaller than during the night. The field strength therewith critically depends on the characteristic size a. For example, at $a = 100$ km the maximal field strength $E_r^{\max}$ is more than an order of magnitude larger than $E_r^{\max}$ at $a = 20$ km and nearly three times smaller than $E_r^{\max}$ at $a = 200$ km both for day and night conditions. The dependence of E_r on r is characterized by a fast initial increase and slow decrease after reaching maximum. The absolute value of $E_r^{\max}$ even for $a = 200$ km at night is only 0.07 mV m^{-1} for $E_0 = 100$ V m^{-1}, i.e. the efficiency of electric field penetration into the ionosphere is low.

Thus, the electric field strength produced by an atmospheric source at ionospheric altitudes is noticeable only when the region of horizontal localization of the field E_z near the Earth's surface is sufficiently wide ($a \geqslant 100$ km) and $E_0 \geqslant 500 - 1000$ V m^{-1}. Our model presented in the previous section confirms the possibility of existence of such a source.

4.2 Ionospheric effect in the E-region

Figure 7 shows the calculated electron concentrations N_e as a function of distance r for three altitudes $z = 115$, 125, and 135 km. For a positive direction of E_z near the Earth's surface N_e decreases above the localization region of E_z (Fig. 7a) and the minimum value occurs at $r = 0$. With $E_z < 0$, i.e. when the field near the surface of the Earth is directed downward, the electron concentration above the localization area increases reaching a maximum at $r = 0$ (Fig. 7b). Thus the effect of the electrostatic field is most pronounced in the middle part of the nocturnal E-region. This is due to the fact that the Pedersen drift V_r is maximal just at these altitudes.

4.3 Metallic ion layer formation

The calculation of the ionospheric effect in the previous case was carried out without taking metallic ions M^+ into account. However, ionospheric plasma in the E-region can have such ions as an additive [28]. Let us consider the effect of the electric field E_r in this case, i.e. assuming that, in addition to molecular ions NO^+, N_2^+, and O_2^+ which are ordinarily the main ions in the E-region, the ionospheric plasma may also contain metallic ions M^+ with a mean mass close to that of molecular ions.

Let us consider the case when the vertical electrostatic field E_z is directed downward onto the base plane. With such a directed field E_z, the radial field component E_r at ionospheric levels and correspondingly the Pedersen ion drift are directed towards the z-axis, which provides the condition of ionospheric plasma storage above the electrostatic field generation region.

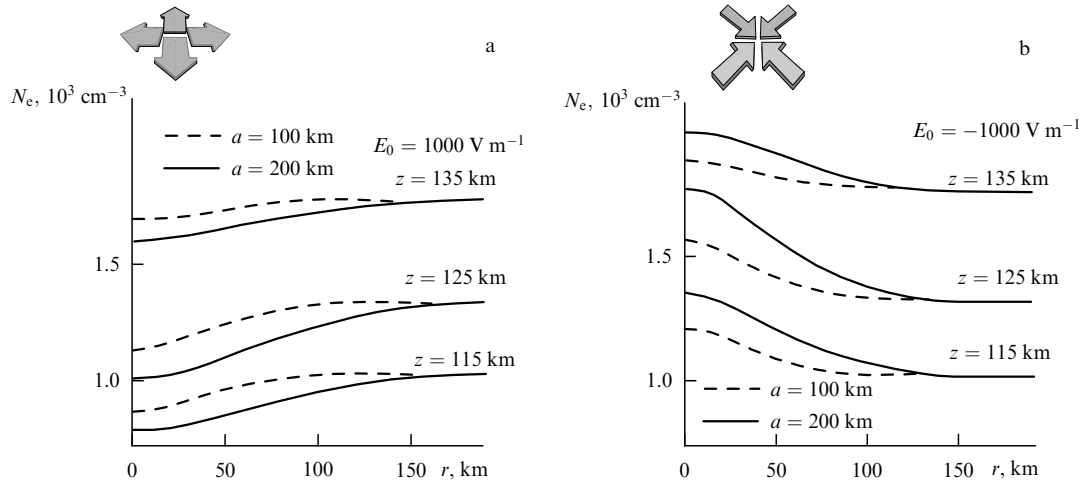

Figure 7.

The results of calculations for $E_0 = -1000$ V m^{-1} and $a = 200$ km are shown in Fig. 8. Before the moment of 'turning-on' the electric field, as well as at the boundary $r = 1500$ km, the molecular and metallic ion concentrations are determined using a photochemical approximation. As seen from the figure, 2 h after the beginning of the action of the electric field the metallic ion concentration above the field generation region becomes higher than for molecular ions in the altitude range 112 – 134 km, and after 4 h the metallic ions dominate at altitudes of 107 – 146 km. Then at altitudes near $z = 120$ km a maximum of the metallic ion concentration occurs reaching 2.5×10^4 cm^{-3} within 4 h, which is approximately 60 times as high as the corresponding initial unperturbed value $N(M^+)$. In contrast, the molecular ion concentration at the same altitudes decreases, and by the moment of 'switching-off' the field a deep minimum of $N(XY^+)$ forms there with a value of 1.0×10^2 cm^{-3}, i.e. $N(XY^+)$ drops by an order of magnitude relative to its initial level.

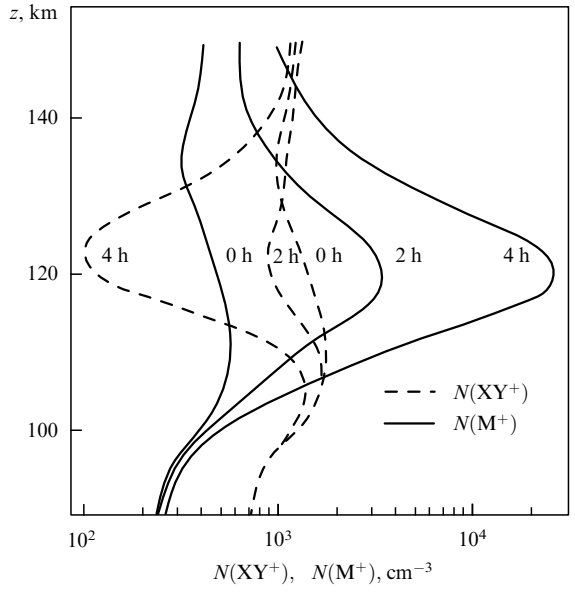

Figure 8.

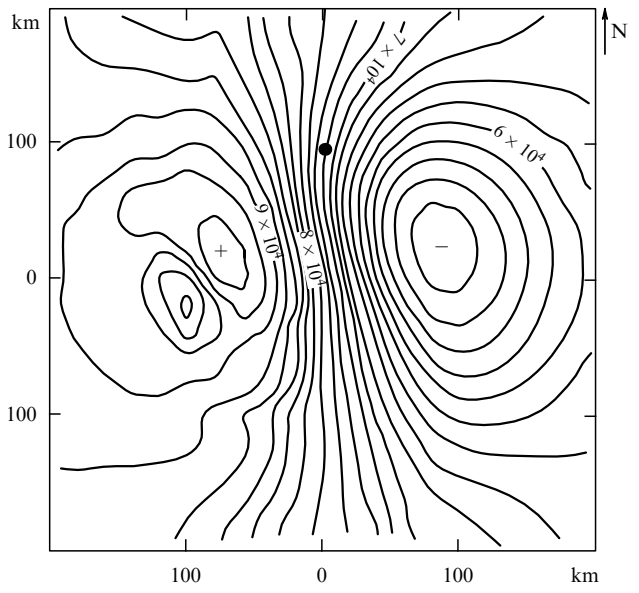

Figure 9.

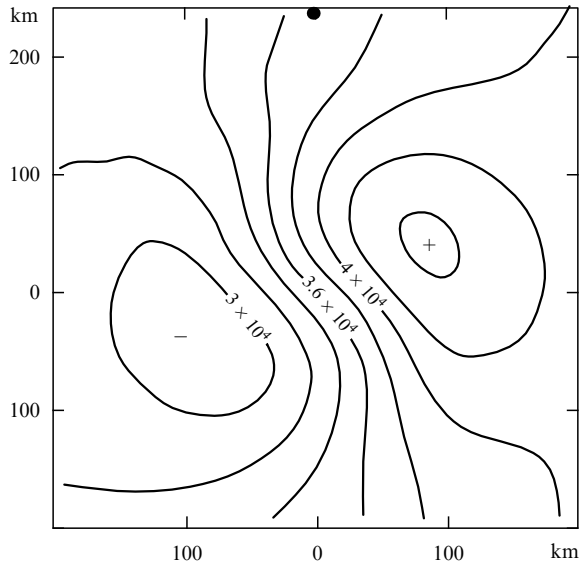

Figure 10.

4.4 Ionospheric effect in the F2-region

To calculate the electric field effect in the nocturnal moderate-latitude F2-region of the ionosphere, we use the ion distribution at altitude $z = 90$ km obtained in Section 4.1. In the cylindrical reference frame (r, φ, z) with the origin on the base plane, $z_0 = 0$, the angle φ is counted counterclockwise outward from the equator (see Fig. 4). Note that at this ionospheric level the electric field has a radial direction relative to the z-axis and is axially symmetric.

As a result of the electrodynamic drift induced by this field, plasma at F2-region altitudes will move along quasi-circular trajectories around the geomagnetic force line z' crossing the z-axis at $z = 90$ km. The force line z' is a line of zero electric field.

In Figures 9, 10, the isolines of constant N_e at altitudes $z = 250$ and 500 km are shown at the moment 2 h after 'turning-on' the field. The black circle marks the vertical projection of the electric field's source centre on the corresponding ionospheric level. As seen from these figures, under the action of the field the horizontal distribution of ionospheric plasma over the F2-region above the field localization region on the base plane becomes essentially nonuniform. The characteristic size of the perturbed region exceeds 400 km. The maximum change in plasma concentration relative to the unperturbed level is about 30% at $z = 250$ km and 20% at $z = 500$ km.

The picture of the horizontal distribution of the ionospheric plasma concentration is characterized by two sharp foci of positive and negative perturbations of N_e. With altitude, the perturbation region of the ionospheric plasma concentration shifts as a whole from the centre of the vertical field localization region on the base plane ($z_0 = 0$) towards the equator. In this way in the bottom part of the F2 ionospheric region, the plasma concentration west and east of the magnetic meridian going through the epicentre increases and decreases, respectively, while in the upper part of the F2-region and at altitudes near the main ionospheric maximum the situation is the opposite: the focus of the positive perturbation of N_e lies east of the geomagnetic

meridian, and west for the negative perturbation. In the case where the vertical electric field E_z on the base plane ($z_0 = 0$) is directed downward, the picture of N_e isolines looks like that shown in Figs 9, 10, but mirror-reflected relative to the magnetic meridian. The strongest change occurs in the bottom part of the F2-region, where inhomogeneities of different size (from 150 to 10 km) are formed with time.

It should be noted that the theoretical description presented here is valid for high and medium latitudes. A special consideration is required for low latitudes and the equator.

5. Discussion of experimental results obtained from land-based and satellite studies of the ionosphere

Ionospheric changes are ordinarily thought to be short-term ($\leqslant 4$ h) variations of electron density and other ionospheric parameters, which arise in quiet conditions without a visible external cause, i.e. in the absence of geomagnetic and other perturbations. The suggested mechanism of influence of atmospheric electricity on the ionosphere allows us (at least partially) to explain this phenomenon. In particular, seismic activity alone strongly affects the ionosphere: variations in the ionosphere of the order of 10–30% start emerging ~ 5 days before an earthquake with magnitude > 5. On average, ~ 300 thousand earthquakes occur on the Earth each year, $\sim 100-120$ of them with magnitude $\geqslant 5$ in different regions of the world. Thus, the Earth's ionosphere turns out to be under the steady influence of seismic activity.

As an example, compare the variations of radon concentration measured in a well near the epicentre of a forthcoming earthquake (Nazarbek, 12 December 1980, $M = 4.7$) and the changes of the critical frequency foF2 measured at an ionospheric station (Tashkent), as shown in Fig. 11 (values averaged over 5-day intervals are shown for fixed moments of local time: 3, 6, and 18 h LT). As seen from Fig. 11, a strong correlation of these parameters confirms the feasibility of the mechanism proposed by us for electric field generation in the presence of an ionization source affecting the ionosphere.

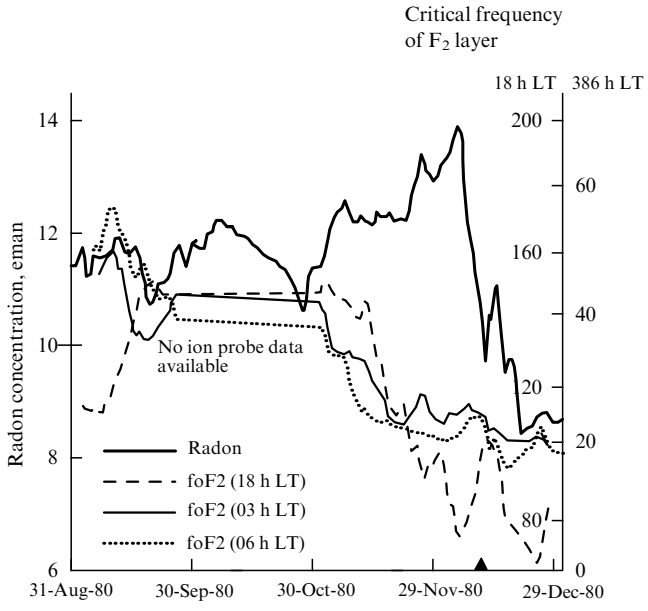

Figure 11.

Experimental evidence is also available for electric field effects at different ionospheric levels. Figure 12 demonstrates a sporadic layer formed at an altitude of ~ 120 km due to the eruption of the Karymskii volcano (Kamchatka) on May 12, 1970 [4], which exactly corresponds to the model calculations presented in Section 4.3. Even more compelling support for the approach considered is the comparison of ionospheric plasma density distributions obtained experimentally with the model calculations presented in Section 4.4. These distributions were found by different methods (land-based and space probing of the ionosphere) and for different physical phenomena (earthquakes and a nuclear power station accident). Figure 13 shows the deviation of the critical frequency foF2 (electron concentration $\sim \sqrt{f\text{oF2}}$) obtained with a land-based network of ionospheric stations 5 days before a strong earthquake in Abruzzo (central Italy) on 07.05.84 with a magnitude of 5.8. A two-foci structure has been discovered which, as in the calculations, is shifted to south relative to the epicentre of the forthcoming earthquake. Similar structures are found when probing ionospheric regions above the areas of the forthcoming earthquake when probing the ionosphere with artificial Earth's satellites [29, 30].

The calculations show that a radioactive injection into the atmosphere strengthens the atmospheric electric field more than above an earthquake region and the efficiency of the electric field penetration is higher, since the radioactive cloud is formed at altitudes of 1–2 km and not on the surface, as prior to an earthquake. In Figure 14, the distribution of the critical frequency change in the F2 ionospheric layer is shown a few hours after the accident at the 'Three Mile Island'

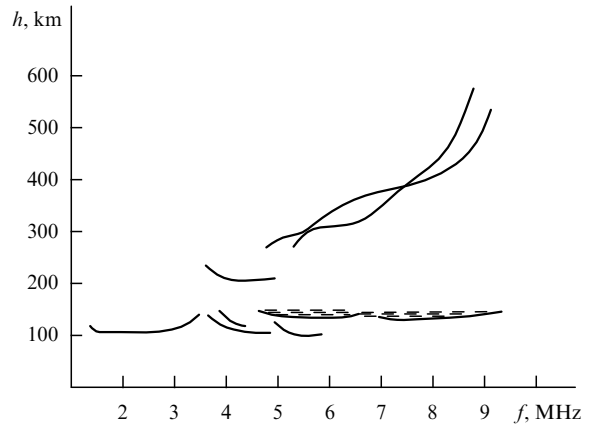

Figure 12.

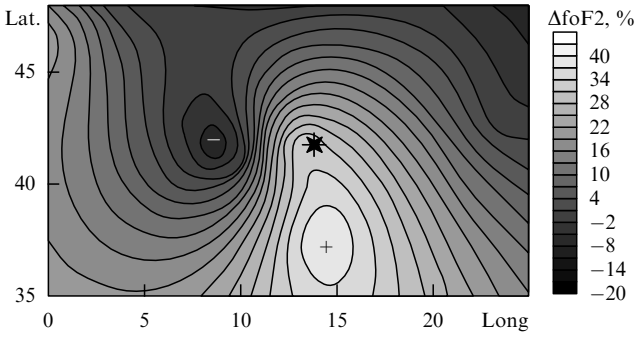

Figure 13.

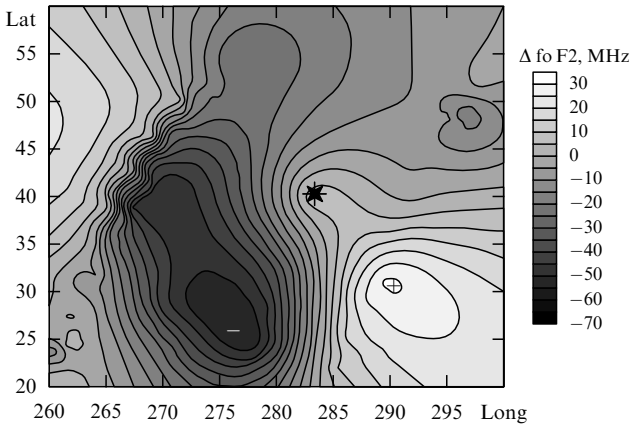

Figure 14.

nuclear power station in the USA, obtained from the IK-19 satellite.

The experimental data presented confirm the results of theoretical predictions and permit us to conclude that the atmospheric electric field is a very important source of ionospheric variations.

6. Conclusions

It was shown that electric field perturbations on the Earth's surface and in the atmosphere can induce changes in the terrestrial ionosphere, the effect of ionospheric variations.

The sources of the atmospheric electric field are atmospheric anomalies (thunder storms, typhoons, atmospheric fronts, etc.), dust and sand storms, large tectonic breaks and seismoactive regions, volcanos, radioactive ejections into the atmosphere during atomic power plant accidents, atmospheric contaminants above big industrial cities, etc.

A self-consistent model is constructed for the electrodynamic interaction between the terrestrial atmosphere and the ionosphere. Specifically, the following results were obtained:

— The anomalous electric field generation on the Earth's surface and in the atmosphere was calculated. It was shown that the additional flux of metallic aerosols leads to anomalous field strengthening.

— The penetration into the ionosphere of an electric field generated in a local region inside the near-surface atmospheric layer was evaluated. The efficiency of field penetration during the night is found to be higher than during day time and to strongly depend on the size of the vertical field (E_z) localization region. The electric field strength at ionospheric altitudes is significant only for large-scale sources on the condition that the maximum $|E_z|$ is about 1000 V m^{-1}.

— The effect of the electric field on the background ionosphere of E- and F-regions was studied. The character of ionospheric perturbations is determined by the direction of E_z.

— A dense layer of metallic ions can be formed under the action of the field above its localization area in the middle part of the nocturnal E-region, which differs from the ordinary middle-latitude sporadic layer E_s by its thickness which is about three times greater than the mean thickness of the E-layer.

— In the picture of the horizontal distribution of the perturbed plasma concentration at altitudes of F2 ionospheric layer two regions with enhanced and decreased concentration are clearly visible. These regions are shifted towards the equator relative to the localization zone centre of the vertical field E_z on the base plane ($z_0 = 0$). The shift increases with altitude.

The mechanism suggested is of a universal character and allows us to explain a whole class of both natural phenomena and anthropogenic influences on the Earth's atmosphere.

A principal possibility appears for using global satellite monitoring of the ionosphere for ecological control and forecasting of anthropogenic catastrophes.

The work was carried out with the financial support of the Russian Fund for Basic Research under grant No 97-05-96620.

References

1. Mitra A, in *Vozdeĭstvie Solnechnykh Vspyshek na Ionosferu* (Effect of Solar Flashes on the Earth Ionosphere) (Moscow: Mir, 1997) p. 370
2. Pulinets S A, in *Proc. International Workshop on Seismo Electromagnetics* (Chofu: University of Electro-Commun. Publ., Japan, 1997) p. 208
3. Boskova J et al. *Stud. Geophys. Geod.* **38** 213 (1994)
4. Kolokolov L E, Shalagina N A, in *Issledovaniya po Geomagnetizmu i Problemam Aéronomii v Vysokikh Shirotakh* (Studies in Geomagnetism and Problems of Aeronomy at High Latitudes) (Magadan: USSR Acad. Sci., Far-East Scientific Centre, 1978) p. 76
5. Fett W *Der Atmosphärische Staub* (Berlin: Deutscher Verlag der Wissenschaften, 1958) [Translated into Russian (Moscow: Inostrannaya Literatura, 1961) p.76]
6. Kamra A K *J. Geophys. Res.* **77** 5856 (1972)
7. Gilbert J S, Lane S J, in *Proc. First International Symposium on Volcanic Ash and Aviation Safety* (U.S. Geological Survey Professional paper 2047, 1994) p. 31
8. Smirnov V V, in *Ionizatsiya v Troposfere* (Ionization in Troposphere) (St. Petersburg: Gidrometeoizdat, 1992) p. 312
9. Nikipelov B V, Drozhko E G *Priroda* (5) 48 (1990)
10. Bonchkovskiĭ V F *Proc. of Geophysical Institute* **25** (152) 192 (1954)
11. Vershinin E F et al., in *Int. Workshop on Seismo Electromagnetics* (March 3 – 5, 1997, Tokyo) p. 23
12. Alekseev V A, Alekseeva N G *Nucl. Geophys.* **6** (1) 99 (1992)
13. Alekseev V A, Alekseeva N G, Jchankuliev J *Radiat. Meas.* **25** (1 – 4) 637 (1995)
14. Roffman A *J. Geophys. Res.* **77** (30) 5883 (1972)
15. Crozier W D *J. Geophys. Res.* **70** (12) 2785 (1965)
16. Boyarchuk K A et al. *BRAS Physics/Suppl. Phys. Vibrations* **60** (4) 236 (1996)
17. Boyarchuk K A *Izv. Ross. Akad. Nauk: Fiz. Atmos. Okeana* **33** (2) 236 (1997)
18. Boyarchuk K A, Svirko Yu P *Pis'ma Zh. Tekh. Fiz.* **22** (14) 47 (1996) [*Tech. Phys. Lett.* **22** 575 (1996)]
19. Hoppel W A *J. Atm. Terrest. Phys.* **29** 709 (1967)
20. Boyarchuk K A, Lomonosov A M, Pulinets S A *BRAS Physics/Suppl. Phys. Vibrations* **61** (3) (1997)
21. *Atmosfera: Spravochnik (Spravochnye Dannye, Modeli)* (Atmosphere: A Handbook (Data, Models) (Leningrad: Gidrometeoizdat, 1991) p. 510
22. Morozov V I *Proc. GGO* (474) 67 (1984)
23. Hoppel W A *J. Geophys. Res.* **90** (D4) 5917 (1985)
24. Wilson C T R, in *Some Thundercloud Problems* (J. Franklin Inst., 1929) (208) p. 12
25. Farley D T, Jr. *J. Geophys. Res.* **64** (9) 1225 (1959)
26. Park C G, Dejnakarintra M *J. Geophys. Res.* **78** (28) 6623 (1973)
27. Cole R K, Jr., Pierce E T *J. Geophys. Res.* **70** (12) 2735 (1965)
28. Kim V P, Khegaĭ V V, Illich-Svitych P V *Geomagnetizm Aéronomiya* **33** (5) 114 (1993)
29. Pulinets S A et al. *Adv. Space Res.* **20** (11) 2173 (1997)
30. Pulinets S A *Adv. Space Res.* **22** (6) 123 (1998)